Microscopy and Microanalysis (2021), **27**, 1498–1505
doi:10.1017/S1431927621012642

Microscopy AND Microanalysis

Original Article

Measuring System Calibration Factors by Unmixing the Excitation–Emission Spectra of One Dish of Cells

Han Sun[1,2], Ao Yin[1,2], Lu Gao[1,2], Hongce Chen[1,2], Qilin Tang[1,2], Ye Yuan[1,2], Zhi Liu[1,2], Zhengfei Zhuang[1,2,3*] and Tongsheng Chen[1,2,3*]

[1]Key Laboratory of Laser Life Science & Institute of Laser Life Science, College of Biophotonics, South China Normal University, Guangzhou 510631, China; [2]Guangdong Provincial Key Laboratory of Laser Life Science, College of Biophotonics, South China Normal University, Guangzhou 510631, China and [3]SCNU Qingyuan Institute of Science and Technology Innovation Co., Ltd., Qingyuan 511517, China

Abstract

Accurate predetermination of the quantum yield ratio (Q_A/Q_D) and the extinction coefficient ratio (K_A/K_D) between acceptor and donor is a prerequisite for quantitative fluorescence resonance energy transfer (FRET) imaging. We here propose a method to measure K_A/K_D and Q_A/Q_D by measuring the excitation–emission spectra (ExEm-spectra) of one dish of cells expressing m ($\geq$3) kinds of FRET constructs. The ExEm-spectra images are unmixed to obtain the weight maps of donor (W_D), acceptor (W_A), and acceptor sensitization (W_S). For each cell, the frequency distribution plots of the W_S/W_D and W_S/W_A images are fitted by using a single-Gaussian function to obtain the peak values of W_S/W_D (SD) and W_S/W_A (SA). The statistical frequency-SD/SA plots from all cells are fitted by using a multi-Gaussian function to obtain the peak values of both SD and SA, and then the ranges of W_S/W_D (R_{SD}) and W_S/W_A (R_{SA}) for each FRET construct are predetermined. Based on the predetermined R_{SD} and R_{SA} values of FRET constructs, our method is capable of automatically classifying cells expressing different FRET constructs. Finally, the W_S/W_D–W_A/W_D plot from different kinds of cells is linearly fitted to obtain K_A/K_D and Q_A/Q_D values.

Key words: acceptor–donor pair, excitation–emission spectra, extinction coefficient ratio, linear spectral unmixing, quantum yield ratio

(Received 16 June 2021; revised 22 July 2021; accepted 13 August 2021)

Introduction

Fluorescence resonance energy transfer (FRET) microscopy based on fluorescent proteins (FPs) has become an important tool for studying molecular dynamics in living cells (Butz et al., 2016; Algar et al., 2019; Wang et al., 2019; Vanderhoof et al., 2020). Quantitative FRET signal, independent of the detection system and the expression level of FPs, is an inevitable requirement for academic exchanges (Ma et al., 2019; Mo et al., 2020; Skruzny et al., 2020; Yang et al., 2020). Quantitative FRET measurement based on linear unmixing of excitation–emission spectra (ExEm-spFRET) has the inherent ability to overcome both acceptor excitation crosstalk and donor emission crosstalk (Hoppe et al., 2013; Mustafa et al., 2013; Du et al., 2016). ExEm-spFRET with as few as two excitation wavelengths makes it easy to perform microscopic ExEm-spFRET imaging for single living cells. Our recent studies have demonstrated the strong robustness of ExEm-spFRET imaging (Lin et al., 2018; Su et al., 2019). We recently also performed an ExEm-unmixing-based FRET two-hybrid assay in living cells to analyze the stoichiometric information of macromolecular complexes (Zhang et al., 2019).

Accurately predetermining the acceptor–donor quantum yield ratio (Q_A/Q_D) and the acceptor–donor extinction coefficient ratio (K_A/K_D) is the prerequisite for quantitative ExEm-spFRET imaging (Mustafa et al., 2013; Du et al., 2016; Zhang et al., 2018; Su et al., 2019). Most FRET-related researches directly cited the quantum yield values of fluorophores reported in the literature to obtain Q_A/Q_D values (Wlodarczyk et al., 2008; Elder et al., 2009; Mustafa et al., 2013). However, in reality, the Q_A/Q_D value of a FRET measurement system is related to not only the optical properties of the donor and acceptor fluorophores but also the intracellular environment of the fluorophores and the spectra response of the measurement system. K_A/K_D is related to the spectra properties of the excitation light source, the transmission function of the measurement system, and the absorption spectra of the donor and acceptor (Wlodarczyk et al., 2008; Elder et al., 2009; Mustafa et al., 2013). Q_A/Q_D and K_A/K_D are constant for a given FRET fluorophore pair and measurement system. We recently proposed a method to measure the Q_A/Q_D and K_A/K_D values simultaneously by using four dishes of cells expressing tandem constructs with different FRET efficiencies (E) and the same acceptor–donor concentration ratio (R_C) (Zhang et al., 2018). This method needs to perform ExEm-spectra imaging for four dishes of cells, which is cumbersome to operate, and cannot guarantee the same image contrast and background signal for different dishes cells.

***Corresponding authors**: Zhengfei Zhuang, E-mail: zhuangzf@scnu.edu.cn; Tongsheng Chen, E-mails: chentsh126@163.com and chentsh@scnu.edu.cn

Cite this article: Sun H, Yin A, Gao L, Chen H, Tang Q, Yuan Y, Liu Z, Zhuang Z, Chen T (2021) Measuring System Calibration Factors by Unmixing the Excitation–Emission Spectra of One Dish of Cells. *Microsc Microanal* **27**, 1498–1505. doi:10.1017/S1431927621012642

In this report, we propose an improved method to measure Q_A/Q_D and K_A/K_D values by imaging only one dish of cells expressing m kinds of different FRET tandem constructs. The cells expressing each one of the different kinds of FRET constructs are mixed into one dish which is performed ExEm-spectra imaging. The measured ExEm-spectra image is then unmixed to get the weight map of donor (W_D), acceptor (W_A), and donor–acceptor sensitization (W_S). Finally, the W_S/W_D–W_A/W_D plot of different kinds of cells is linearly fitted to obtain K_A/K_D and Q_A/Q_D. Based on the predetermined ranges of W_S/W_D (R_{SD}) and W_S/W_A (R_{SA}) of each FRET constructs, our method is capable of automatically classifying the cells expressing different FRET constructs in one dish and thus makes it possible to perform the automatic measurement of the Q_A/Q_D and K_A/K_D values by one-click operation.

Method and Materials

Cell Culture, Tandem FRET Constructs, and Transfection

Cell lines Hela were obtained from the Cell Bank of the Chinese Academy of Sciences (Shanghai, China) and cultured in Dulbecco's Modified Eagle's Medium (DMEM, Gibco, Grand Island, NE, USA) supplemented with 10% fetal bovine serum (FBS, Sijiqing, Hangzhou, China) and 1% penicillin and streptomycin (Gibco, Grand Island, NE, USA) in CO_2 incubators (Thermo Fisher, USA).

Cerulean (C) and Venus (V) were purchased from Addgene Company (Cambridge, MA, USA), and CTV, C32V, C17V, and C5V constructs were kindly provided by the Vogel Lab (National Institutes of Health, Bethesda, Maryland) (Thaler et al., 2005; Koushik et al., 2009).

For transfection, Hela cells were first cultured in the four wells of a six-well plate, and each well contained 1 mL DMEM. CTV, C32V, C17V, and C5V were transfected, respectively, into the four wells of cells for 4–6 h by using Lipofectamine 2000 (Invitrogen, Carlsbad, CA, USA). The cells in the four wells were then detached and subsequently mixed into a 35-mm glass dish and cultured for 12–24 h in CO_2 incubators (Yin et al., 2021).

Theory and Measurement Steps

Theory

The ExEm-spectra signatures of the donor (S_D), acceptor (S_A), and donor–acceptor sensitization (S_S) are the outer product of the excitation spectra (S_X^{ex}, $X = D$ and A) and the emission spectra (S_X^{em}, $X = D$ and A) measured from donor-only and acceptor-only samples, respectively, as follows (Zhang et al., 2018):

$$\begin{aligned} S_D &= S_D^{ex} \otimes S_D^{em} \\ S_A &= S_A^{ex} \otimes S_A^{em} \\ S_S &= S_D^{ex} \otimes S_A^{em}. \end{aligned} \quad (1)$$

The ExEm-spectra image (S_{DA}) of a FRET sample is linearly separated into three parts as follows:

$$S_{DA} = W_D \cdot S_D + W_S \cdot S_S + W_A \cdot S_A, \quad (2)$$

where W_D, W_S, and W_A are the contributions of the S_D, S_S, and S_A in S_{DA}, respectively. We also obtain (Du et al., 2016; Zhang et al., 2018; Su et al., 2019; Zhang et al., 2019)

$$\frac{W_S}{W_D} = \frac{K_D}{K_A} \cdot \frac{W_A}{W_D} - \frac{Q_A}{Q_D}, \quad (3)$$

where Q_A/Q_D is the acceptor–donor quantum yield ratio, and K_A/K_D is the acceptor–donor extinction coefficient ratio.

For different FRET tandem constructs with different FRET efficiencies (such as CTV, C32V, C17V, and C5V), measure their $W_{A\text{-}i}/W_{D\text{-}i}$ and $W_{S\text{-}i}/W_{D\text{-}i}$ ratios (Fig. 1a), and perform a linear fitting according to equations (3) to obtain the K_A/K_D (the reciprocal of the slope of the linear equation) and Q_A/Q_D (the absolute value of the intercept) of the imaging system (Fig. 1b).

Measurement Steps

Cells (test sample) expressing different FRET tandem constructs, cultured in a 35-mm glass dish, are used for measuring Q_A/Q_D and K_A/K_D, which includes the following three steps:

Step 1: predetermining the ranges of W_S/W_A (R_{SA}) and W_S/W_D (R_{SD}) of each FRET tandem construct.

a. The ExEm-spectra image of the test sample is segmented into M independent cells. For the ith segmented cell ($i = 1, 2, 3,\ldots, M$), the ExEm-spectra images ($S_{DA\text{-}i}$) are unmixed according to equation (2) to obtain the three weight images ($W_{D\text{-}i}$, $W_{S\text{-}i}$, and $W_{A\text{-}i}$), and the corresponding $W_{S\text{-}i}/W_{A\text{-}i}$ and $W_{S\text{-}i}/W_{D\text{-}i}$ ratio images and frequency distribution histogram plot are fitted by a single-Gaussian function. The Gaussian peak values of $W_{S\text{-}i}/W_{A\text{-}i}$ and $W_{S\text{-}i}/W_{D\text{-}i}$ are denoted as $SA_{\text{-}i}$ and $SD_{\text{-}i}$, respectively.
b. The SA and SD frequency distribution histogram plots for the M cells are fitted by multi-Gaussian (m-Gaussian, m is the number of the FRET tandem construct species used for test) function, and the SA and SD Gaussian peaks are recorded as $P_{SA\text{-}1}$, $P_{SA\text{-}2},\ldots$, $P_{SA\text{-}m}$ and $P_{SD\text{-}1}$, $P_{SD\text{-}2},\ldots$, $P_{SD\text{-}m}$, respectively.
c. The $R_{SA\text{-}m}$ and $R_{SD\text{-}m}$ of the mth kind of FRET tandem constructs are defined as $P_{SA\text{-}m} \pm \delta_{Am}$ and $P_{SD\text{-}m} \pm \delta_{Dm}$, and the δ_{Am} and δ_{Dm} values are defined according to the m-Gaussian function fitting.

Step 2: Classification of cells expressing different FRET tandem constructs.

a. For a test sample, the ExEm-spectra image is unmixed to obtain the SA and SD *images* according to equation (2).
b. Generating m kinds of classification masks according to SA and SD *images*: for a pixel, if the SA *is* in $R_{SA\text{-}j}$ and SD *is* in $R_{SD\text{-}j}$ ($j = 1, 2,\ldots, m$), the pixel value is set to 1; otherwise, it is set to 0, and the corresponding mask is denoted as $CM_{\text{-}j}$.
c. The cells are divided into m kinds of cells by using the $CM_{\text{-}1}$, $CM_{\text{-}2},\ldots, CM_{\text{-}m}$ masks, respectively, to filter the W_S/W_D and W_A/W_D *images* and calculate the corresponding statistical value for each kind of cells.

Step 3: Linearly fitting the W_S/W_D–W_A/W_D plot for the m kinds of FRET tandem constructs to obtain K_A/K_D and Q_A/Q_D according to equations (3) (Fig. 1b).

ExEm-Spectra Imaging

ExEm-spectra imaging was performed on a self-built ExEm-spectra FRET microscope which consists of a wide-field microscope (IX73, Olympus, Tokyo, Japan) equipped with a motorized cube wheel (IX3-RFACA, Olympus), a motorized emission filter wheel (FW103, Thorlabs, Newton, New Jersey, USA) with six positions in total, an sCMOS camera (Flash 4.0, Hamamatsu Photonics k.k., Hamamatsu, Japan), a 40×/1.30 objective (Olympus), and a mercury lamp (HGLGPS, Olympus). The excitation filter (Ex 436/20 nm and Ex 470/20 nm, Chroma,

https://doi.org/10.1017/S1431927621012642 Published online by Cambridge University Press

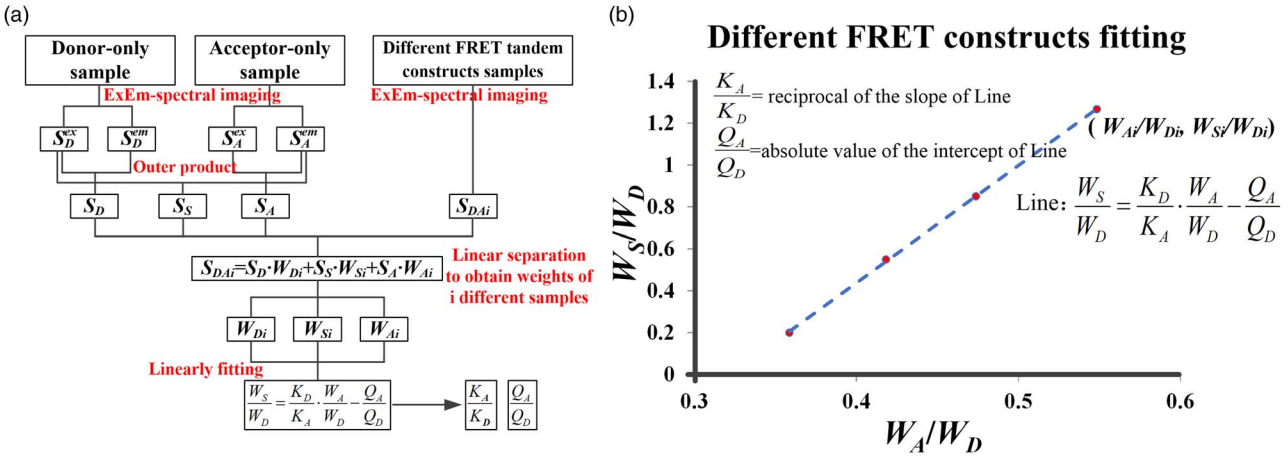

Fig. 1. (**a**) Diagram of measuring K_A/K_D and Q_A/Q_D. (**b**) Plot of W_S/W_D–W_A/W_D for linearly fitting to obtain K_A/K_D and Q_A/Q_D. The reciprocal of the slope of the line is K_A/K_D, and the absolute value of the intercept is Q_A/Q_D.

Vermont, USA) was set in the cube wheel, and the emission filter (Em 470/20 nm, Em 490/20 nm, Em 510/20 nm, Em 530/20 nm, and Em 550/20 nm, Chroma, Vermont, USA) was set in the emission filter wheel (Supplementary Fig. 1).

Results and Discussion

Predetermining the Ranges of W_S/W_D (R_{SD}) and W_S/W_A (R_{SA}) Values

First, cells separately expressing C or V were used to measure their ExEm-spectra (S_D, S_A, and S_S) through the outer product of their normalized ExEm-spectra (Supplementary Fig. 2). Figure 2 shows the process how to predetermine the R_{SD} and R_{SA} ranges of CTV, C32V, C17V, and C5V constructs by using one dish of cells. Cells transfected separately with CTV, C32V, C17V, or C5V construct for 5 h in a six-well plate were combined into one dish and then were cultured for 12 h before ExEm-spectra imaging. Figure 2a shows the ExEm-spectra images of the dish of cells, which were unmixed to obtain the pseudo-color images of W_S/W_A and W_S/W_D according to equation (2) (Fig. 2b). The cell circled by a red box in Figure 2b was performed pixel-by-pixel frequency distribution histogram plots of W_S/W_A and W_S/W_D values (blue dots, Fig. 2c) and a single-Gaussian function fitting (red line, Fig. 2c), exhibiting peak values: SD = 0.94 and SA = 1.64. We performed a similar single-Gaussian function fitting for the frequency-W_S/W_A and frequency-W_S/W_D histograms of 589 cells in the dish of cells and plotted SA and SD frequency distribution histogram (Fig. 2d) which was fitted by using a four-Gaussian function fitting. The four-Gaussian peak values are $P_{SD\text{-}CTV} = 0.10$, $P_{SD\text{-}C32V} = 0.60$, $P_{SD\text{-}C17V} = 0.90$, and $P_{SD\text{-}C5V} = 1.30$; $P_{SA\text{-}CTV} = 0.15$, $P_{SA\text{-}C32V} = 1.40$, $P_{SA\text{-}C17V} = 1.90$, and $P_{SA\text{-}C5V} = 2.30$. Eventually, we predetermined the range of both R_{SD} and R_{SA} for each FRET construct as following (Fig. 2e): $R_{SD} \sim (0.05, 0.15)$ and $R_{SA} \sim (0.1, 0.2)$ for CTV; $R_{SD} \sim (0.5, 0.7)$ and $R_{SA} \sim (1.35, 1.55)$ for C32V; $R_{SD} \sim (0.8, 1.0)$ and $R_{SA} \sim (1.8, 2.0)$ for C17V; and $R_{SD} \sim (1.2, 1.4)$ and $R_{SA} \sim (2.2, 2.4)$ for C5V.

Twice Gaussian fittings are used to predetermine the ranges of R_{SA} and R_{SD}. A single-Gaussian function fitting is first performed to obtain the peak values of SA and SD for each cell (Fig. 2c), and then a four-Gaussian function fitting is performed for the frequency-peak histograms of SA and SD from all cells to classify the cells expressing different kinds of constructs (Fig. 2d), and finally, the R_{SA} and R_{SD} ranges of each FRET tandem construct were determined according to the four-Gaussian function fitting (Fig. 2e). The obtained R_{SA} and R_{SD} ranges are very stable and accurate by using twice Gaussian fittings. In reality, we also directly performed the plots of frequency-W_S/W_A (Supplementary Fig. 3a) and frequency-W_S/W_D (Supplementary Fig. 3b) for the same 589 cells, and we only clearly determined two Gaussian peaks, and the other peaks were buried, which lead to inaccurate cell classification.

It is obvious that the narrower the ranges of R_{SD} and R_{SA}, the more accurate the cell classification. However, too narrow ranges of R_{SD} and R_{SA} must leave out many cells, which is not conducive to subsequent fitting. For predetermining more accurate R_{SD} and R_{SA}, we hope that each FRET construct has a high expression level, and their FRET efficiency has significant differences. Moreover, we also hope that as many cells as possible are imaged, ensuring the number of cells expressing different types of FRET tandem constructs meets the statistical criteria. For a dish of cells, it is difficult to ensure that different FRET constructs have similar transfection efficiency and expression level, thus the numbers of cells expressing different FRET tandem constructs are not controllable. There are two rules for predetermining R_{SD} or R_{SA}: (1) avoiding the R_{SD} / R_{SA} ranges across of different FRET tandem constructs; (2) R_{SD} or R_{SA} of different FRET tandem constructs should be as large as possible. In reality, we counted 589 cells in one dish containing 184 cells expressing CTV, 287 cells expressing C32V, 65 cells expressing C17V, and 53 cells expressing C5V. We determined R_{SD} and R_{SA} (Fig. 2e) by using twice Gaussian fitting. In reality, the number of the cells expressing C17V or C5V was significantly less than that of the cells expressing C32V or CTV in the same image field, which may be due to the insufficient detachment of the C17V or C5V cells from the six-well plate compared with the CTV cells and C32V cells. Although the difference in the number of each kind of construct cells does not influence our R_{SD} or R_{SA} results, it is better to improve the experimental technique to control the considerable number of various FRET construct cells. We strongly recommend that cells had better reach 90% of the well plate before transfection, and the cells sufficiently detached from the well plate need to be centrifuged after finish transfection before they are fully mixed to ensure cells evenly spread in a 35-mm glass dish.

https://doi.org/10.1017/S1431927621012642 Published online by Cambridge University Press

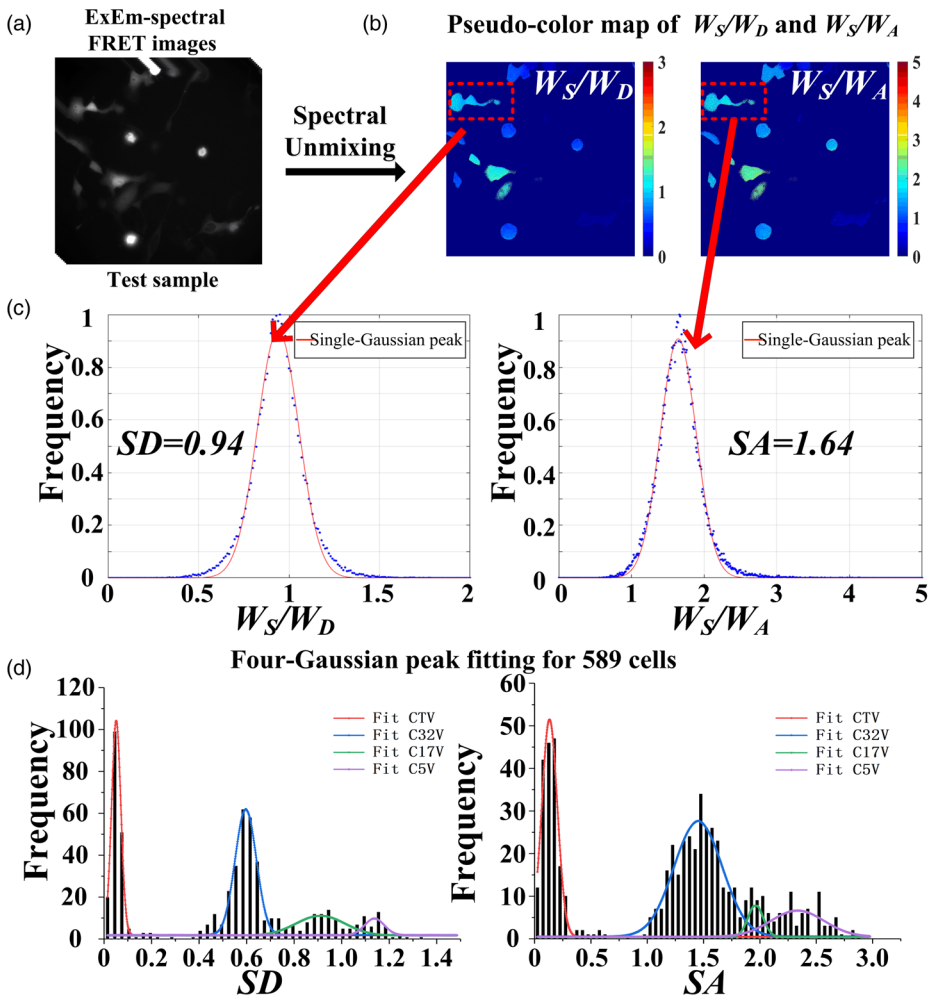

(e)

Constructs	CTV	C32V	C17V	C5V
R_{SD}	(0.05,0.15)	(0.5,0.7)	(0.8,1.0)	(1.2,1.4)
R_{SA}	(0.1,0.2)	(1.35,1.55)	(1.8,2.0)	(2.2,2.4)

Fig. 2. Predetermining the R_{SD} and R_{SA} for CTV, C32V, C17V, and C5V constructs, respectively. (**a**) ExEm-spectra images of one dish of cells expressing four kinds of FRET tandem constructs. (**b**) Pseudo-color images of the W_S/W_D and W_S/W_A obtained by unmixing the ExEm-spectra images (**a**). (**c**) Single-Gaussian function fitting of the frequency distribution of W_S/W_D and W_S/W_A for the cell indicated by red box in (**b**) to obtain its SD and SA values. (**d**) Four-Gaussian function fitting for the frequency-SD and frequency-SA plots from 589 cells, including 184 CTV cells, 287 C32V cells, 65 C17V cells, and 53 C5V cells. The red line indicates CTV; the blue line indicates C32V; the green line indicates C17V; and the purple line indicates C5V. (**e**) R_{SD} and R_{SA} values of four kinds of FRET constructs.

Accurate cell segmentation is necessary for predetermining the ranges of R_{SD} and R_{SA}. Due to the very small distances between adjacent cells, a cell mask may contain a few different FRET tandem construct cells, which must result in an inaccurate Gaussian fitting. In reality, we found that background filtering threshold was very important for accurate cell segmentation. We defined a threshold β factor to characterize the effect of different background filtering threshold on cell segmentation. β *I_{BG} (background gray level) was used as the threshold value that was deducted from the original image (I_{raw}) to obtain $I_{raw} - \beta$ *I_{BG} image which was then binarized (let pixels less than 0 equal to 0, and let pixels greater than 0 equal to 1) to obtain mask (I_{mask}). As shown in the red box of Figure 3a, the cell outline of the connected areas becomes finer and finer by increasing β from 1 to 2.5, and five cells can be perfectly segmented when β = 2.5. However, there are still some overlapping cells that cannot be effectively segmented by increasing β in the blue box. In reality, most of the connected regions can be segmented appropriately in the case of β = 1.6. For a connected cell, the adjusted R^2 coefficient (Marchal-bressenot et al., 2015) was used to evaluate the accuracy of Gaussian fitting. For performing the single-Gaussian function fitting, the closer value of adjusted R^2 is to 1, the more accurate the Gaussian fitting. As shown in the first line of Figure 3b, we performed a single-Gaussian function fitting on the connected regions of overlapping cells (blue box of Fig. 3a, β = 2.5), and the adjusted R^2 values obtained from the fitting results of W_S/W_A and W_S/W_D are 0.30 and 0.38, respectively, indicating this area contains different cells expressing with different constructs.

https://doi.org/10.1017/S1431927621012642 Published online by Cambridge University Press

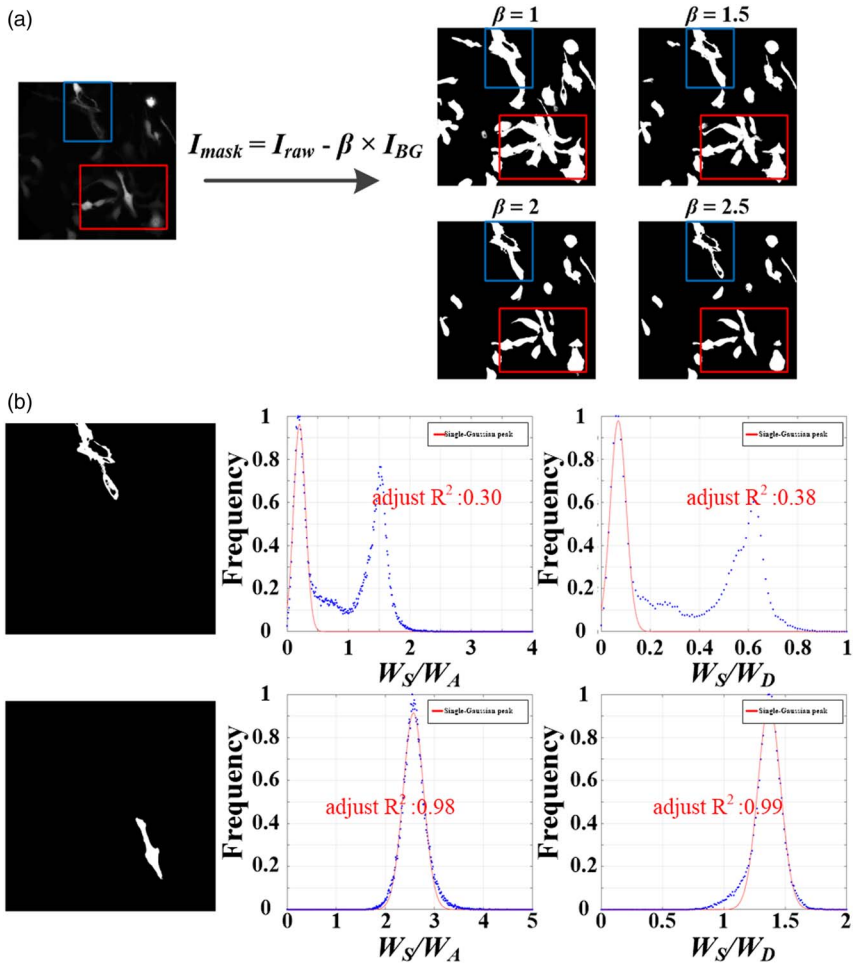

Fig. 3. Effect of background filtering threshold on cell segmentation. (**a**) Cell segmentation with different background filtering threshold. Left: original cell image expressing four kinds of FRET tandem constructs in one dish. Right: masks obtained by subtracting different threshold from the original image. (**b**) Cell segmentation and adjusted R^2 values. First line: left, cell mask (blue box of (**a**), $\beta = 2.5$); Middle and right: frequency distribution histogram plots of W_S/W_A and W_S/W_D values (blue dots) and single-Gaussian function fitting (red line), the adjusted R^2 values are 0.30 and 0.38, respectively. Second line: left, cell mask (one region of red box of (**a**), $\beta = 2.5$); Middle and right: frequency distribution histogram plots of W_S/W_A and W_S/W_D values (blue dots) and single-Gaussian function fitting (red line), the adjusted R^2 values are 0.98 and 0.99, respectively.

In contrast, as shown in the second line of Figure 3b, the adjusted R^2 values of a segmented cell in the red box of Figure 3a ($\beta = 2.5$) are 0.98 and 0.99, respectively, indicating the effective single-cell segmentation. We took the adjusted R^2 value greater than 0.95, as the prerequisite of a connected cells area can be segmented into a single-cell segmentation level to ensure the accuracy of the predetermined R_{SD} and R_{SA} values.

Measure K_A/K_D and Q_A/Q_D by Using One Dish of Cells

After the cells transfected separately with CTV, C32V, C17V, or C5V for 5 h were combined into one dish and then cultured for 12 h, we performed ExEm-spectra imaging. Figure 4a shows the ExEm-spectra images of a representative field, which was linearly separated according to equation (2) to obtain W_D, W_A, and W_S, and the corresponding W_A/W_D, W_S/W_D (SD), and W_S/W_A (SA) images (Fig. 4b). We next produced four cell classification masks according to the SD and SA images. According to Figure 2e, for a pixel, if the SD is in (0.05, 0.15) and the *SA* is in (0.1, 0.2), the pixel value of the mask was set as 1, otherwise as 0, obtaining CTV cell classification mask (CTV mask) (Fig. 4c). Similarly, we also obtained C32V mask, C17V mask, and C5V mask (as shown in Fig. 4c). Next, we used the four masks to filter the raw W_S/W_D and W_A/W_D images, respectively, and obtained the filtered W_S/W_D and W_A/W_D images (Fig. 4d). Nineteen cells were recognized in this representative field, including four CTV cells, eight C32V cells, five C17V cells, and two C5V cells. For this field, $W_{S\text{-}CTV}/W_{D\text{-}CTV} = 0.069$ and $W_{A\text{-}CTV}/W_{D\text{-}CTV} = 0.359$; $W_{S\text{-}C32V}/W_{D\text{-}C32V} = 0.607$ and $W_{A\text{-}C32V}/W_{D\text{-}C32V} = 0.418$; $W_{S\text{-}C17V}/W_{D\text{-}C17V} = 0.902$ and $W_{A\text{-}C17V}/W_{D\text{-}C17V} = 0.474$; and $W_{S\text{-}C5V}/W_{D\text{-}C5V} = 1.266$ and $W_{A\text{-}C5V}/W_{D\text{-}C5V} = 0.548$. We linearly fitted the W_S/W_D–W_A/W_D plot and obtained $K_{A11}/K_{D11} = 1/6.18$ and $Q_{A11}/Q_{D11} = 2.07$ (Fig. 4e). We selected 45 ExEm-spectra imaging fields, and the average fitting results of four FRET constructs are shown in Figure 4f, obtaining $K_{A1}/K_{D1} = 1/6.70$ and $Q_{A1}/Q_{D1} = 2.33$.

In generating classification masks from W_S/W_D and W_S/W_A images, we also evaluated the effect of signal-to-noise ratio (S/N ratio) on our method. In reality, cells with S/N ratios greater than 1.6 are filtered pixel-by-pixel. For example, for the cell indicated by red box in Supplementary Figure 4a, the W_S/W_D, W_S/W_A, and W_A/W_D images are uniform (Supplementary Fig. 4b)

https://doi.org/10.1017/S1431927621012642 Published online by Cambridge University Press

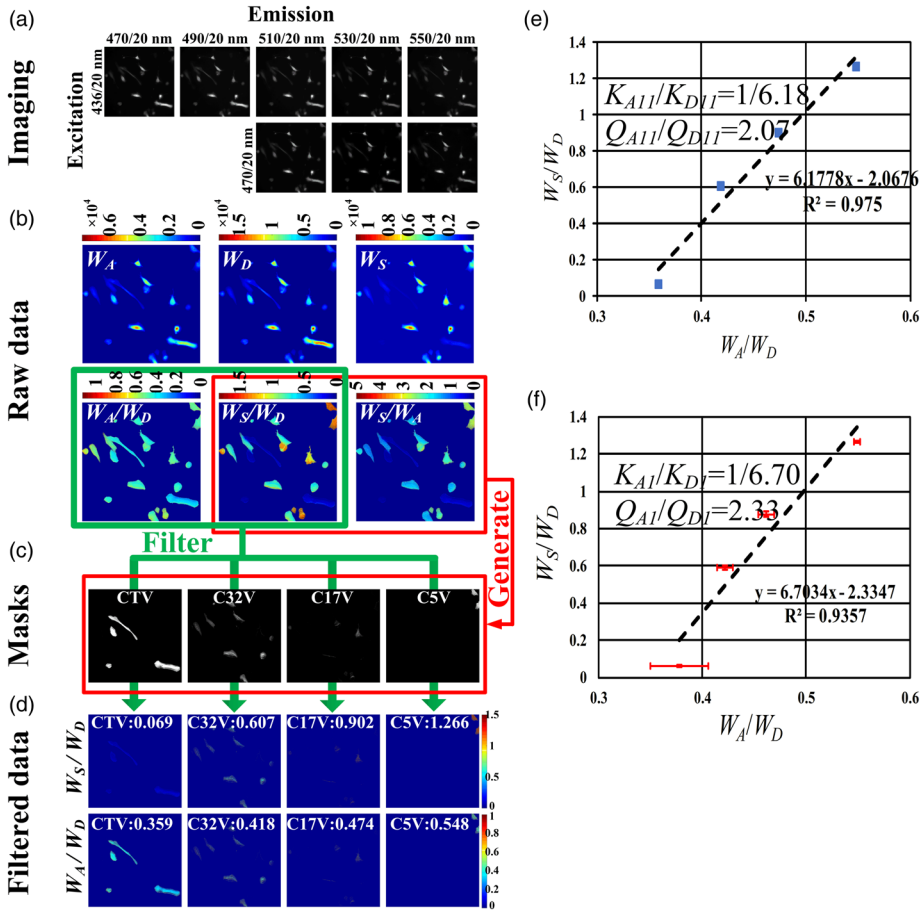

Fig. 4. K_A/K_D and Q_A/Q_D measurement by unmixing the ExEm-spectra of a dish of cells expressing CTV, C32V, C17V, and C5V. (**a**) ExEm-spectra images of one dish of cells expressing the four kinds of constructs. (**b**) W_D, W_A, W_S, and the corresponding *Raw* SD and SA images. (**c**) CTV, C32V, C17V, and C5V masks. (**d**) Filtered W_S/W_D and W_A/W_D images by using the masks. (**e**) Linearly fitting the W_S/W_D–W_A/W_D plot from (**d**) and obtain K_A/K_D = 1/6.18 and Q_A/Q_D = 2.07 of (**a**). (**f**) Linearly fitting the W_S/W_D–W_A/W_D plot from 45 ExEm-spectra imaging fields and obtain K_{A1}/K_{D1} = 1/6.70 and Q_{A1}/Q_{D1} = 2.33.

but the corresponding S/N ratio images are from 1.6 to 25 (Supplementary Fig. 4c), indicating that W_S/W_D, W_S/W_A, and W_A/W_D are independent of S/N ratio in this S/N ratio ranges. Next, pixels were divided into two kinds of pixels ($1.6 < S/N < 5$ and $S/N > 5$) to further evaluate the influence of the S/N ratio on the measured results. In the case of $1.6 < S/N < 5$, the measured result is $K_A/K_{D(1.6<S/N<5)} = 1/6.412$ and $Q_A/Q_{D(1.6<S/N<5)} = 2.174$, consistent with the $K_A/K_{D(S/N>5)} = 1/6.315$ and $Q_A/Q_{D(S/N>5)} = 2.069$ in the case of $S/N > 5$, further indicating that S/N ratio greater than 1.6 has no effect on the measured K_A/K_D and Q_A/Q_D values.

Anomalous CTV Construct

We found that after cell filtering by classification masks, the W_A/W_D value range of CTV is larger than other FRET constructs. The fitting results using three constructs (C32V, C17V, and C5V) without CTV are shown in Figure 5b, obtaining $K_{A2}/K_{D2} = 1/5.13$ and $Q_{A2}/Q_{D2} = 1.54$. We measured the E_D and R_C values of C17V with two sets of correction factors and compared them with the values reported in the literature (Koushik et al., 2006, 2009; Koushik & Vogel, 2008) as shown in Figure 5c. The E_D value calculated by using $Q_{A2}/Q_{D2} = 1.54$ is 0.39, consistent with the literature value (Koushik et al., 2006), while the E_D value calculated by using 2.33 of Q_{A1}/Q_{D1} is 0.29, significantly lower than the literature value (0.38) (Koushik et al., 2006). The calculated R_C value by using the K_{A2}/K_{D2} and K_{A1}/K_{D1}, respectively, is close to 1 (Fig. 5c). We also calculated the E_D and R_C values of cells expressing C32V, C17V, and C5V by using the $K_{A2}/K_{D2} = 1/5.13$ and $Q_{A2}/Q_{D2} = 1.54$ and obtained consistent results with the values reported in the literature (Figs. 5d, 5e) (Koushik et al., 2006).

The facts that the E_D value of C17V measured by using K_{A1}/K_{D1} and Q_{A1}/Q_{D1} obtained by using C32V, C17V, C5V, and CTV constructs is 0.28, much lower than the 0.39 (the expected value is 0.38) measured by using K_{A2}/K_{D2} and Q_{A2}/Q_{D2} obtained by using C32V, C17V, and C5V constructs further demonstrate the Coulomb's opinion that the tendency of the C–V linker of CTV is forming trimers, thereby bringing the fluorophores in close contact causing energy transfer from C to several V acceptors (Coullomb et al., 2020). Therefore, CTV is unsuitable for our method.

Conclusion

In this report, we propose a method to measure the system calibration factors (K_A/K_D and Q_A/Q_D) by spectrally imaging only one dish of cells expressing m ($m \geq 3$) kinds of FRET tandem constructs. Because of imaging only one dish of cells to complete the measurement of K_A/K_D and Q_A/Q_D, our method bypasses the influence of different contrast and background signals during

https://doi.org/10.1017/S1431927621012642 Published online by Cambridge University Press

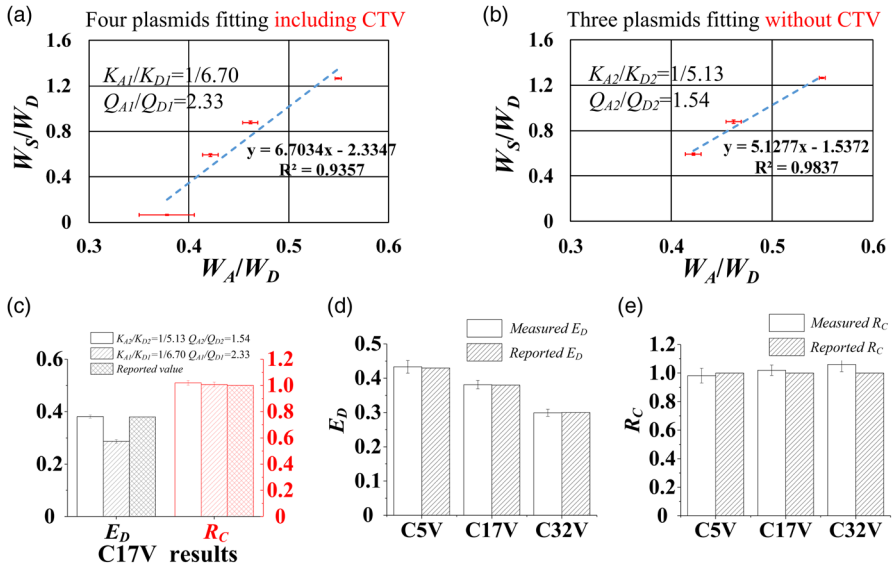

Fig. 5. A negative influence of CTV construct. (**a**) Linearly fitting the W_S/W_A–W_A/W_D plot from the four FRET constructs including CTV, C32V, C17V, and C5V, and obtain the correction factors K_{A1}/K_{D1} = 1/6.70 and Q_{A1}/Q_{D1} = 2.33. (**b**) Linearly fitting the W_S/W_A–W_A/W_D plot from the three FRET constructs including C32V, C17V, and C5V, and obtain the correction factors K_{A2}/K_{D2} = 1/5.13 and Q_{A2}/Q_{D2} = 1.54. (**c**) E_D and R_C results of the C17V cells by using two sets of K_A/K_D and Q_A/Q_D values. (**d,e**) E_D (**d**) and R_C (**e**) values of three constructs calculated by using the K_{A2}/K_{D2} = 1/5.13 and Q_{A2}/Q_{D2} = 1.54.

ExEm-spectra imaging. In addition, our method is capable of automatically classifying cells expressing different FRET constructs, making it possible to realize the automatic measurement of K_A/K_D and Q_A/Q_D by one-clink operation. It is worth noting that our experiment further proves the abnormality of CTV which is unsuitable for our method. Therefore, our method provides a solid basis to realize automatic ExEm-spectra imaging and system calibration, thereby lowing the threshold of live-cell FRET imaging, furthermore paving the way of developing an intelligent FRET correction system.

Supplementary material. To view supplementary material for this article, please visit https://doi.org/10.1017/S1431927621012642.

Acknowledgments. The authors thank Prof. S. S. Vogel (HIN/NIAAA) for providing CTV, C32V, C17V, and C5V constructs. This work is supported by the National Natural Science Foundation of China (NSFC) (Grant Nos. 61875056 and 62135003) and the Science and Technology Program of Guangzhou (Grant No. 2019050001).

References

Algar WR, Hildebrandt N, Vogel SS & Medintz IL (2019). FRET as a biomolecular research tool—Understanding its potential while avoiding pitfalls. *Nat Methods* **16**, 815–829. doi:10.1038/s41592-019-0530-8

Butz ES, Ben-Johny M, Shen M, Yang PS, Sang L, Biel M, Yue DT & Wahl-Schott C (2016). Quantifying macromolecular interactions in living cells using FRET two-hybrid assays. *Nat Protoc* **11**, 2470–2498. doi:10.1038/nprot.2016.128

Coullomb A, Bidan CM, Qian C, Wehnekamp F, Oddou C, Albigès-Rizo C, Lamb DC & Dupont A (2020). QuanTI-FRET: A framework for quantitative FRET measurements in living cells. *Sci Rep* **10**, 6504. doi:10.1038/s41598-020-62924-w

Du M, Zhang L, Xie S & Chen T (2016). Wide-field microscopic FRET imaging using simultaneous spectral unmixing of excitation and emission spectra. *Opt Express* **24**, 16037–16051. doi:10.1364/OE.24.016037

Elder AD, Domin A, Kaminski Schierle GS, Lindon C, Pines J, Esposito A & Kaminski CF (2009). A quantitative protocol for dynamic measurements of protein interactions by Förster resonance energy transfer-sensitized fluorescence emission. *J Royal Soc Interface* **6**, S59–S81. doi:10.1098/rsif.2008.0381.focus

Hoppe AD, Scott BL, Welliver TP, Straight SW & Swanson JA (2013). N-way FRET microscopy of multiple protein-protein interactions in live cells. *PLoS One* **8**, e64760. doi:10.1371/journal.pone.0064760

Koushik SV, Blank PS & Vogel SS (2009). Anomalous surplus energy transfer observed with multiple FRET acceptors. *PLoS One* **4**, e8031. doi:10.1371/journal.pone.0008031

Koushik SV, Chen H, Thaler C, Puhl HL 3rd & Vogel SS (2006). Cerulean, Venus, and VenusY67C FRET reference standards. *Biophys J* **91**, L99–L101. doi:10.1529/biophysj.106.096206

Koushik SV & Vogel SS (2008). Energy migration alters the fluorescence lifetime of Cerulean: Implications for fluorescence lifetime imaging forster resonance energy transfer measurements. *J Biomed Opt* **13**, 031204. doi:10.1117/1.2940367

Lin F, Du M, Yang F, Wei L & Chen T (2018). Improved spectrometer-microscope for quantitative fluorescence resonance energy transfer measurement based on simultaneous spectral unmixing of excitation and emission spectra. *J Biomed Opt* **23**, 1–10. doi:10.1117/1.JBO.23.1.016006

Ma L, Jongbloets B, Xiong W, Zhong H & Mao T (2019). Imaging neuromodulatory signaling events at single cell resolution in behaving animal. *Microsc Microanal* **25**(S2), 1130–1131. doi:10.1017/S143192761900638X

Marchal-Bressenot A, Salleron J, Boulagnon-Rombi C, Bastien C, Cahn V, Cadiot G, Diebold MD, Danese S, Reinisch W, Schreiber S, Travis S & Peyrin-Biroulet L (2015). Development and validation of the Nancy histological index for UC. *Gut* **66**, 43–49. doi:10.1136/gutjnl-2015-310187

Mo GCH, Posner C, Rodriguez EA, Sun T & Zhang J (2020). A rationally enhanced red fluorescent protein expands the utility of FRET biosensors. *Nat Commun* **11**, 1848. doi:10.1038/s41467-020-15687-x

Mustafa S, Hannagan J, Rigby P, Pfleger K & Corry B (2013). Quantitative Förster resonance energy transfer efficiency measurements using simultaneous spectral unmixing of excitation and emission spectra. *J Biomed Opt* **18**, 26024. doi:10.1117/1.JBO.18.2.026024

Skruzny M, Pohl E, Gnoth S, Malengo G & Sourjik V (2020). The protein architecture of the endocytic coat analyzed by FRET microscopy. *Mol Syst Biol* **16**, e9009. doi:10.15252/msb.20199009

Su W, Du M, Lin F, Zhang C & Chen T (2019). Quantitative FRET measurement based on spectral unmixing of donor, acceptor and spontaneous excitation-emission spectra. *J Biophotonics* **12**, e201800314. doi:10.1002/jbio.201800314.

Thaler C, Koushik SV, Blank PS & Vogel SS (2005). Quantitative multiphoton spectral imaging and its use for measuring resonance energy transfer. *Biophys J* **89**, 2736–2749. doi:10.1529/biophysj.105.061853

Vanderhoof B, Nelson R, Beiner G, Raicu V & Oliver J (2020). Tissue factor oligomerization in living cells using förster resonance energy transfer. *Microsc Microanal* **26**(S2), 828–829. doi:10.1017/S1431927620015986

Wang S, Shen B, Ren S, Zhao Y, Zhang S, Qu J & Liu L (2019). Implementation and application of FRET-FLIM technology. *J Innov Opt Heal Sci* **12** 1930010. doi:10.1142/S1793545819300106

Wlodarczyk J, Woehler A, Kobe F, Ponimaskin E, Zeug A & Neher E (2008). Analysis of FRET signals in the presence of free donors and acceptors. *Biophys J* **94**, 986–1000. doi:10.1529/biophysj.107.111773

Yang F, Qu W, Du M, Mai Z, Wang B, Ma Y, Wang X & Chen T (2020). Stoichiometry and regulation network of Bcl-2 family complexes quantified by live-cell FRET assay. *Cell Mol Life Sci* **77**, 2387–2406. doi:10.1007/s00018-019-03286-z

Yin A, Sun H, Chen H, Liu Z, Tang Q, Yuan Y, Tu Z, Zhuang Z & Chen T (2021). Measuring calibration factors by imaging a dish of cells expressing different tandem constructs plasmids. *Cytometry A* **99**, 632–640. doi:10.1002/cyto.a.24316

Zhang C, Lin F, Du M, Qu W, Mai Z, Qu J & Chen T (2018). Simultaneous measurement of quantum yield ratio and absorption ratio between acceptor and donor by linearly unmixing excitation-emission spectra. *J Microsc* **270**, 335–342. doi:10.1111/jmi.12687

Zhang C, Liu Y, Qu W, Su W, Du M, Yang F & Chen T (2019). ExEm-FRET two-hybrid assay: FRET two-hybrid assay based on linear unmixing of excitation-emission spectra. *Opt Express* **27**, 18282–18295. doi:10.1364/OE.27.018282

https://doi.org/10.1017/S1431927621012642 Published online by Cambridge University Press